Chapter 12

Textured BST Thin Film on Silicon Substrate: Preparation and Its Applications for High Frequency Tunable Devices

Conchun Zhang, Jianze Huang,
Chunsheng Yang and Guifu Ding

Additional information is available at the end of the chapter

http://dx.doi.org/10.5772/intechopen.79270

Abstract

The dielectric properties of $Ba_{0.5}Sr_{0.5}TiO_3$ (BST) thin films are sensitive to the relative crystallographic orientation of the films. $LaNiO_3$ (LNO) and MgO were deposited as buffer layer on Si substrate before BST. The effect of buffer layer such as LNO, MgO and MgO/LNO bilayer on the microstructure and dielectric properties of BST were extensively investigated. The preferred (100) orientation of LNO by radio frequency (RF) magnetron sputtering was dominated by the substrate temperature and highly (100)-oriented LNO thin films were grown on Si substrates at 300°C. The oriented (100) growth of sputtered BST thin films was strongly affected by the orientation of LNO thin films and the tunability of BST thin film was greatly improved with the insertion of (100)-textured LNO buffer layer. In addition, MgO, as a buffer layer, was deposited by RF magnetron sputtering. The results show that the crystallization of BST was also enhanced by the insertion of MgO buffer layer, which enhances the oriental growth of BST along (100). Also, the tunability of the BST thin films was improved and the dielectric loss greatly decreased. Finally, CPW with BST/MgO multilayer was fabricated and the scattering (S) parameters were tested.

Keywords: magnetron sputtering, BST, oriented growth, buffer layer, dielectric properties, tunability

1. Introduction

Tunable high frequency devices are key components for the next generation of communications and radar systems. Oxides with the perovskite structure, such as barium strontium

titanate (BST), have ferroelectric, high dielectric, high-Tc superconductive or very large magnetron resistance. Therefore, they are widely investigated for applications in the tunable microwave filters and monolithic microwave integrated circuit decoupling capacitors. For application in frequency agile devices, it is desirable to have as large a capacitance change ratio and as low a dielectric loss as possible. Many researches have been studied to increase the tunability and to reduce the loss of epitaxial BST films grown on single crystal oxide substrates, such as $LaAlO_3$ and MgO [1–4]. However, in order to integrate BST thin films with Si for frequency agile devices, it is necessary to deposit BST thin films on Si substrates. But it is difficult to prepare high-quality oxide films on Si due to inherent crystallographic incompatibility of the two materials and the lack of an epitaxial template for the growth of well-oriented $Ba_{1-x}Sr_xTiO_3$ [4].

The dielectric properties of BST thin films are sensitive to the relative crystallographic orientation of the films, usually highly oriented BST film leads to higher performance compared to a randomly oriented one. There are various methods for changing the orientation of the ferroelectric films, such as the insertion of a buffer layer and/or different bottom electrodes [4–6]. Kang et al. reported the physical properties of epitaxial $Ba_{0.6}Sr_{0.4}TiO_3$ (BST) films grown on SiO_2/Si using biaxially oriented MgO as template layers [4]. A buffer layer used between the silicon substrate and the perovskite oxides thin film has been shown to be a good way of overcoming the problem [5, 7–12]. Previous study showed that the dielectric constant of BST thin films was improved by LNO buffer layer [8, 11], where the thin films were prepared by pulsed laser deposition. $LaNiO_3$ (LNO), a perovskite-type metallic oxide, has a lattice parameter of 3.84 Å. The crystal structural and lattice constants of the LNO matches well with ferroelectric thin films such as BST films [5, 10], which offer the benefits of better lattice matching and structural compatibility and the potential for improved dielectric properties. However, some studies showed that the LNO layer hardly affected the texture of BST thin films [13].

On the other hand, MgO shows low microwave loss, good thermal stability and has been increasingly utilized in microwave devices. The crystal parameter of MgO is a = b = c = 0.42 nm, which is close to that of BST (about 0.39 nm). The single crystal MgO has been used as a microwave substrate [14]. However, the high cost of MgO crystal restrains the popularity of massive production [15]. Few works have been reported on MgO thin films deposited by RF magnetron sputtering as a buffer layer for BST [16].

In this chapter, buffer layer such as $LaNiO_3$ thin film or MgO thin film were deposited on silicon substrate by RF magnetron sputtering. Here, both the effect of the sputtering parameters on the orientation of LNO thin film and the effect of the LNO/MgO buffer layer on the microstructure and dielectric properties of sputtered BST were studied [17–21].

2. Experimental details

BST and LNO targets for our experiment were synthesized by conventional sintering process using a conventional mixing oxides method. The LNO films with varied thickness (600–2400 Å), mainly used as a buffer layer, were deposited at room temperature or at 300°C by RF

magnetron sputtering. The substrate was silicon or platinized silicon. The sputtering power was 100 W and the relative O_2 ratio ranged from 10 to 50% with the total pressure of 1.33 Pa. For the LNO deposited at room temperature, the LNO film was post annealed at 700°C for 1 h in O_2 atmosphere for crystallization.

BST thin film was deposited under various relative oxygen ratios with total Ar and O_2 pressure of 0.8 Pa, and then it was post annealed at 700–750°C in O_2 atmosphere for crystallization.

MgO buffer layers were deposited at room temperature on Si wafers. The working pressure is 0.3 Pa, and O_2 partial ratio changed was 10%. The RF magnetron sputtering power is 100 W. The thickness of thin films was measured by a stylus profiler (Veeco Dektak 6M). The thickness of the MgO buffer layer is between 50 and 150 nm. Then, $Ba_{0.5}Sr_{0.5}TiO_3$ thin films were deposited on MgO buffer layers by RF magnetron sputtering. The deposition pressure was 0.8 Pa. Both the MgO and the BST/MgO composite films were annealed in the O_2 atmosphere.

The compositional analysis was performed by induced coupling plasma emission spectroscopy (ICP) using an Iris Advantage 1000 instrument. The phase and crystallinity of the films were characterized by an X-ray diffractometer (XRD) D/MAX-γB, Rigaku with CuKa radiation. Atomic force microscopy (AFM) surface morphologies were achieved with a Digital Instrument Nanoscope III with AFM tapping mode. Then the resistivity was determined by a four-point probe (China, D41-11A/ZM) at room temperature. The microstructure of the thin films was examined by field emission-scanning electron microscopy (FE-SEM). For the measurements of the dielectric properties, the Cu/Cr top electrodes were deposited by sputtering method and were patterned by liftoff technology. The planar capacitor was prepared based on BST/LNO Pt (111)//Ti/SiO_2/Si thin film, and interdigital capacitor was prepared based on BST/MgO/SiO_2/Si thin films. The dielectric properties of the BST films were measured using an HP 4194A impedance analyzer at a frequency of 1 MHz. C-V characteristic was carried out with a sine wave with a 0.1 V step at a frequency of 1 MHz at room temperature.

3. Oriented $LaNiO_3$ or MgO buffer layer on Si for the textured $Ba_{0.5}Sr_{0.5}TiO_3$ thin films

3.1. RF sputtered BST thin film on Si substrate

BST thin films can be deposited by different methods such as hydrothermal, pulsed laser deposition, metal organic chemical vapor deposition (MOCVD), chemical solution deposition method and sol-gel. Among these methods, we chose radio frequency magnetron sputtering technique due to its industrial process compatibility through ease of implementation, superior compositional reproducibility, medium deposition rate, uniform deposition over large area with additional interest in mass production [22–24]. However, transferring the target stoichiometry to the substrate remains a challenge with on-axis RF-magnetron sputtering due to re-sputtering effects. Thus, the control of the re-sputtering and the etch rate are critical issues related to the sputtering of BST thin films. This etch rate is known to be strongly influenced by

the deposition parameters. There have been several reported methods to reduce the impact of this phenomenon. The common method is to use an off-axis deposition [25], where the surface is not parallel to the target surface. Another method is to increase the sputtering gas pressure, providing higher anion-gas collisions to reduce the energy of negative particles or deflecting them away from the film. In the present study, the key to achieve stoichiometric BST thin film deposition was by controlling both target composition and oxygen concentration to avoid the re-sputtering and the substrate etching. BST thin films were deposited by on-axis radio-frequency magnetron sputtering, then the films were annealed at 750°C in O_2 atmosphere.

Figure 1 shows the composition of the BST thin films deposited by on-axis RF-magnetron sputtering in Ar/O_2 mix gas is deviated from the target, which is due to re-sputtering effects, that is, oxygen negative ions bombardment of the growing film. The BST thin films close to stoichiometric composition, $Ba_{0.5}Sr_{0.5}TiO_3$, were sputtered with a $(Ba_{0.8}Sr_{0.8})TiO_3$ target in Ar gas. The re-sputtering effect can be decreased when no oxygen was introduced during sputtering since the re-sputtering phenomenon is attributed to the presence of energetic particles (negative oxygen ions).

As can be seen in **Figure 2**, the BST thin film deposited at room temperature was amorphous. When annealed at 750°C in O_2 atmosphere for 30 min, thin film crystallized. With increasing annealing time, the grain size increased and some large grains appeared. Annealing at 750°C for no more than 30 min is beneficial for the homogenous grain growth.

Figure 3 shows the XRD patterns of the BST thin films on SiO_2/Si deposited in different oxygen ratio (P_{O_2}) and annealed at 750°C for 30 min. BST sputtered in Ar/O_2 mix gas cannot form complete perovskite phase and some non-perovskite phase appears because of oxygen negative ions bombardment of the growing film. But Perovskite phase formed when the BST thin film were sputtered in Ar gas.

Figure 4 shows the C-V characteristic of the BST thin films directly deposited on $Pt/SiO_2/Si$. The curve was asymmetric because the bottom electrode (Pt) and top electrode (Cu) were different. When the bias voltage switched, the two curves were symmetric with x = 0 V as axis of symmetry.

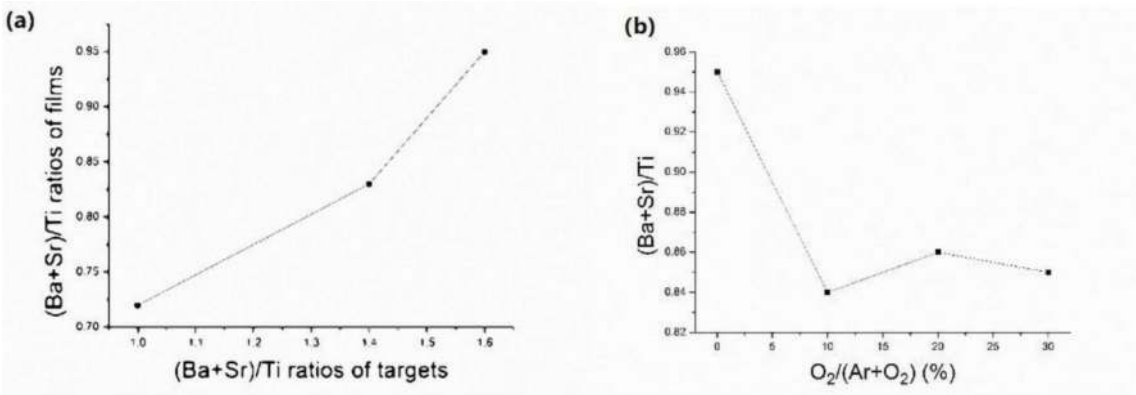

Figure 1. (a) The effect of target composition and (b) P_{O_2} on (Ba + Sr)/Ti ratio of the BST thin films SiO_2/Si (total pressure = 0.8 Pa).

http://dx.doi.org/10.5772/intechopen.79270

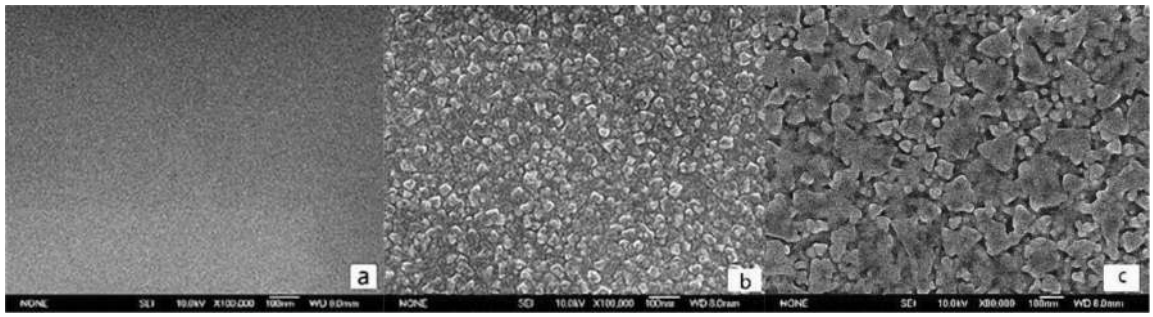

Figure 2. SEM of the BST thin films on SiO_2/Si: (a) as-deposited (b) annealed at 750 in O_2 atmosphere for 30 min and (c) annealed at 750 in O_2 atmosphere for 60 min.

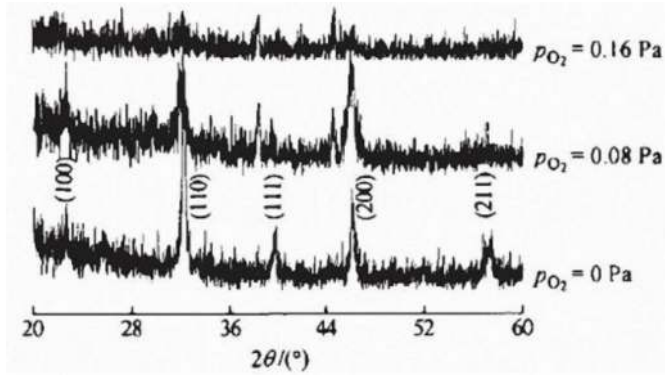

Figure 3. XRD spectra of BST film sputtered under different relative oxygen ratio (P_{O_2}).

3.2. RF sputtered $LaNiO_3$ on Si substrate

As shown in **Figure 5**, the chemical composition analysis by ICP, that is, the La/Ni ratio (mole ratio) in the LNO thin films varied with relative oxygen ratios. The La/Ni ratio keeps stoichiometric ratio of 1:1 while the relative oxygen ratio is between 10 and 25%; however, as the relative oxygen ratio exceeds 25%, the content of La decreases. In the sputtering process, oxygen participated in the sputtering as well as a reaction gas. Because of the energy difference between oxygen ion and argon ion, the change of the relative oxygen ratio will lead to the change of sputtering yield of La and Ni, but the change should be continuous and monotonous. The structure with La/Ni ratio of 1:1 is relatively stable, La and Ni are selectively adsorbed in the film in the process of sputtering, so the component of the film keeps stable when the relative oxygen ratio maintains between 10 and 25%. This indicates that the films tend to grow according to stoichiometric ratio during the sputtering process [26]. **Figure 6** shows the XRD patterns of the LNO films. According to XRD results of **Figure 6a**, the LNO films deposited at room temperature with different relative oxygen ratio and post annealed at 700°C for 1 h show a perovskite-type cubic structure with a random orientation irrespective of O_2 ratio. The full width at half maximum (FWHM) of the (110) peak increases slightly when the O_2 ratio exceeds 25%, that is, the LNO films have better crystalline when the relative oxygen ratio is no more than 25%. The mole ratio of La/Ni for the film deviates from stoichiometric ratio when the O_2 ratio exceeds 25%, therefore, the LNO films deposited above 25% O_2 ratio

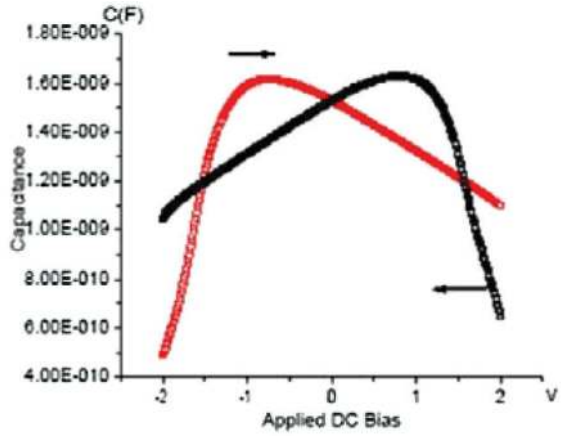

Figure 4. C-V diagram before and after changing the DC bias direction.

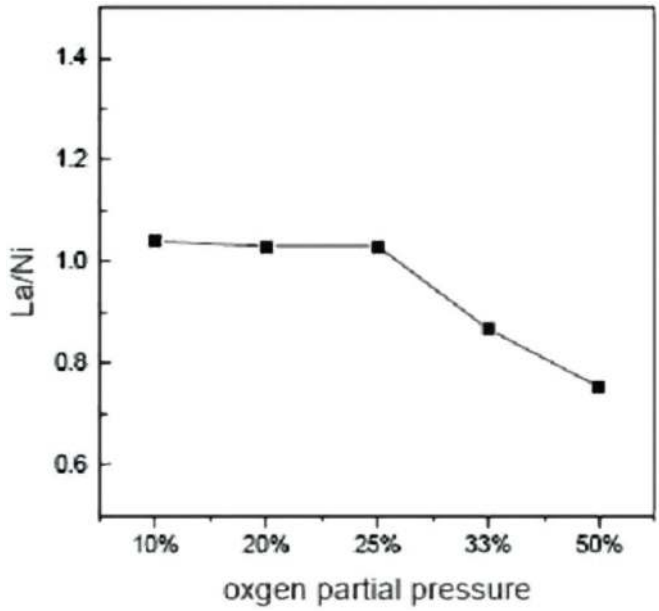

Figure 5. The dependence of La/Ni ratio on the relative oxygen ratio.

show bad crystalline. The surface morphology of the LNO thin films by AFM are summarized in **Table 1**. The mean roughness value of the film deposited with 10% O_2 ratio was 1.5 nm, while the surface roughness value was 5.0 nm and many voids were observed when the O_2 ratio exceeded 25%. **Figure 6(b)** and **(c)** shows the thin films deposited on Pt (111)/SiO_2/Si with 10% oxygen at room temperature and 300°C, respectively. It can be seen that the films show an entirely perovskite phase with a (100) preferential orientation when the LNO thin film was deposited at 300°C (**Figure 6(c)**). However, when the LNO thin film was deposited at room temperature and was post-annealed for crystallization (**Figure 6(b)**), the thin film showed random orientation. Combined the XRD results in **Figure 6(a)–(c)**, it revealed that the

http://dx.doi.org/10.5772/intechopen.79270

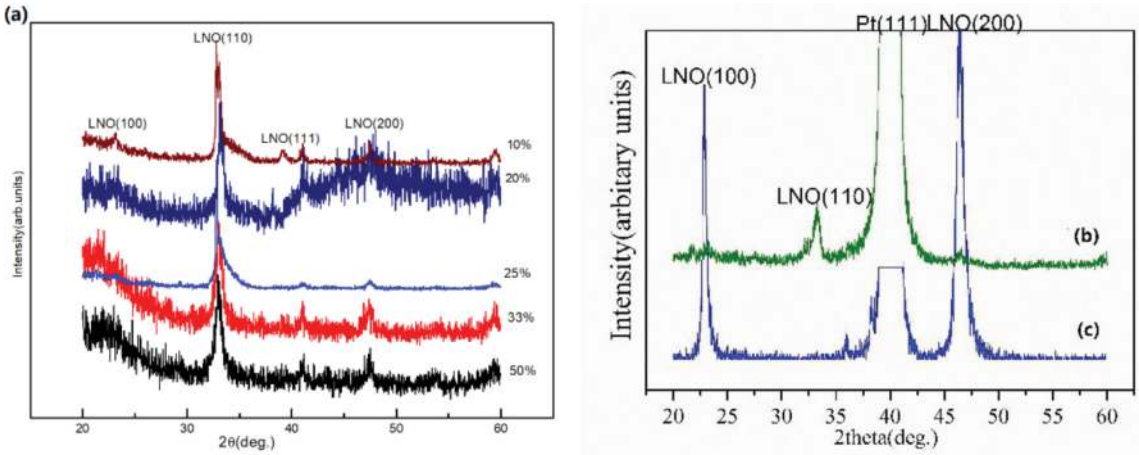

Figure 6. XRD patterns of the LNO thin films. (a) Deposited on SiO_2/Si at room temperature with different oxygen ratios and post annealed at 700°C. (b) Deposited on Pt(111)/SiO_2/Si at room temperature and annealed at 700°C for 1 h with 10% oxygen ratio. (c) Deposited on Pt (111)/SiO_2/Si with 10% oxygen ratio at 300°C.

Oxygen ratios (%)	R_a (nm)	Surface morphology
10	1.5	Smooth
25	2.4	Smooth
33	4.6	Rough, some voids
50	5.0	Many voids

Table 1. The morphology of the LNO films deposited on SiO_2/Si at different oxygen ratios and postannealed at 700°C.

oriented growth of the LNO thin films was dominated by deposition temperature, which was due to the collision between the energetic particles and the thin film during sputtering [12], the detailed discussion was given in Ref [27].

As we know, the preferred orientations of thin films are affected by many parameters. Surface free energies of two-dimensional planes affect the preferred orientation of films in the initial stage of film growth [28]. The film will be oriented to the plane which has the smallest surface free energy if the effect of the substrate is negligible. In ceramic systems with unit cell containing cations and anions, both the electrostatic charges of two-dimensional planes and surface packing densities should be considered in the calculation of surface free energies. It is difficult to find out the surface free energies of ceramics. Furthermore, in RF magnetron sputtering process ionic species ejected from the target surface will also influence the orientations of films. The film orientation can be adjusted by changing the process conditions such as substrate temperature, ambient pressure. In the film deposited at low pressures, the size of the plume was large and the substrate was located at the middle of plume. The kinetic energies of ionic species were higher than those of atomic and molecular species. While the absolute number of ionic species was small, they were absorbed on the substrate preferentially and the influence of electrostatic charges became dominant at the initial stage of film growth. The

kinetic energies of absorbed species were determined by the substrate temperature. When the substrate temperature was high enough, the absorbed species had sufficient energies to rearrange along the plane with the electrically neutral planes, that is, the (100) equivalent planes, therefore textured LNO films were obtained.

The resistivity of LNO measured by four points probe method is shown in **Table 2**. It shows that the resistivity increases rapidly when the O_2 ratio is more than 33%, which can be explained as following: one is the decreased La resulting in the composition deviated from the stoichiometric ratio, another one is that the film contains many voids. This indicates that the films can be deposited at 300°C with O_2 ratio less than 33%. The effects of the relative O_2 ratio, substrate temperatures on the microstructure and electrical properties of the $LaNiO_3$ thin films by RF sputtering have been investigated [26]. It revealed the films deposited at 300°C show (100) preferred orientation. This indicates that the substrate temperature plays an important role in the determination of the films orientation. The LNO films deposited with 10% O_2 ratio had the lowest resistivity and as such be suitable as a buffer layer or electrode of perovskite oxide thin films.

3.3. Textured BST thin film on LNO/Pt/SiO_2/Si (100) substrate

BST thin films were deposited on different electrodes and post annealed in O_2 at 700–750 °C atmosphere for 30 min. **Figure 7(a)–(c)** shows the XRD patterns of BST thin films deposited on different electrodes. The films in **Figure 7b** and **c** show a well-developed perovskite phase without other crystalline phases, but the BST thin films directly deposited on Pt electrode showed relatively weak crystallization compared with those deposited on LNO buffer layer. Mainly oriented (100) peak with small extra (110) peaks, was observed in the BST film deposited on LNO (100)/Pt (111) in **Figure 8b** and **c** [10]. It can be seen that the (100)-textured LNO films due to a good match of lattice parameters between LNO and BST, as well as a similar perovskite structures, further facilitated the crystallization and growth of the BST films. Also, the BST thin film deposited on 120 nm LNO shows better crystallinity than that of the BST film on 60 nm LNO. The AFM images in **Figure 7(d)–(f)** revealed that the surface of BST on Pt shows some white hillocks because Ti can migrate into the surface via Pt grain boundaries and results in the formation of hillocks, and larger grain size is observed in the BST thin films deposited on LNO/Pt (111) compared to that deposited on Pt (111). These results are in agreement with XRD, which means that LNO buffer layers enhance the growth of BST grains. On

Oxygen ratio (%)	Resistivity(MΩ cm) (T_d = 300°C)
10	2.45
20	2.51
33	2.49
50	23.1

Table 2. The resistivity of the LNO thin film sputtered with different O_2 ratios.

http://dx.doi.org/10.5772/intechopen.79270

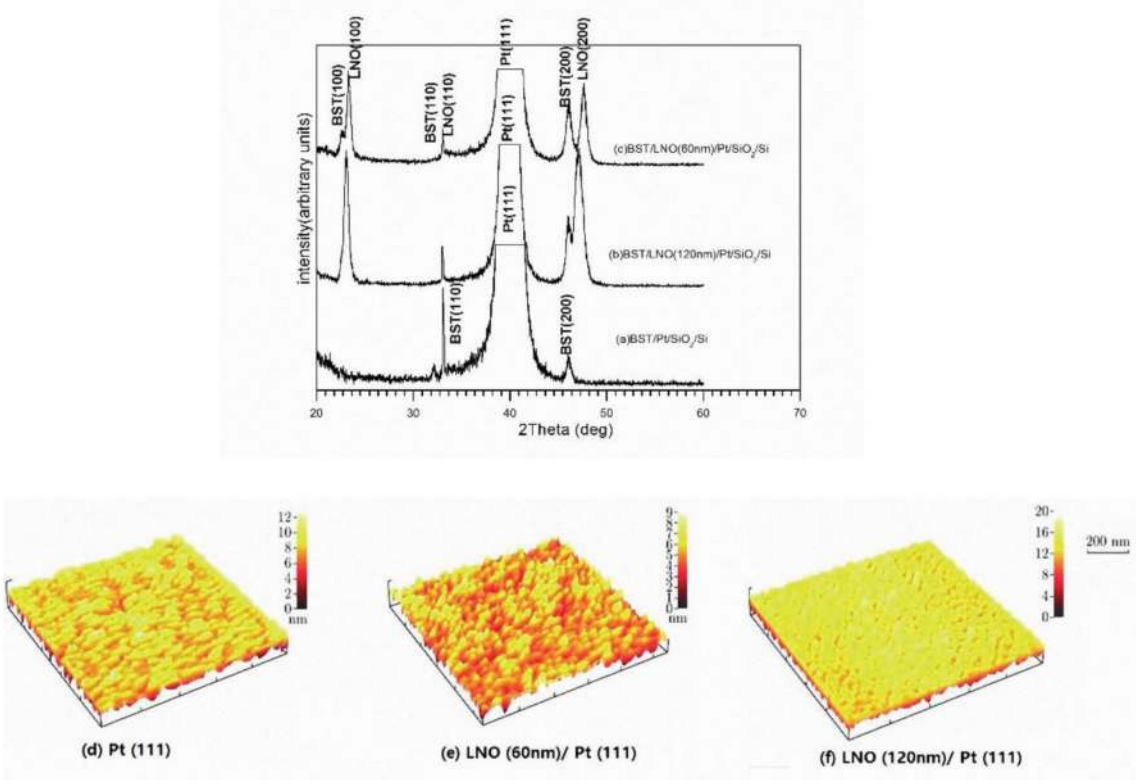

Figure 7. Characterization of BST thin films [30]. (a–c) X-ray diffraction patterns of BST films deposited on various substrates (a) Pt (111), (b) LNO (100) 120 nm/Pt (111), (c) LNO (100) 60 nm/Pt (111); (d–f) AFM surface morphology of the BST thin films deposited on various substrates (d) Pt (111), (e) LNO (100) 120 nm/Pt (111), (f) LNO (100) 60 nm/Pt (111).

the other hand, increasing LNO thickness leads to the rougher surface when the thickness of LNO is more than 60 nm. The root-mean-square (RMS) values of surface roughness of the BST film in **Figure 7(d)–f)** are 7, 5, 8 nm, respectively.

3.4. The dielectric properties of BST multilayer thin films

For the measurements of the dielectric properties, parallel capacitor was prepared. **Figure 8(1)** shows the structure of BST capacitor and **Figure 8(2)** shows the dielectric properties of the BST thin films varied with the electric field. The asymmetric C-V curves may arise from the difference between bottom electrode and top electrode [29]. The tunability of the ferroelectric film can be expressed with the equation as following:

$$\text{Tunability} = \frac{C_{max} - C_{min}}{C_{max}} \tag{1}$$

According to Eq. (1), the tunability of BST thin films on the LNO (100)/Pt (111) and on the LNO (110)/Pt (111) were about 63 and 50% at 500 kV/cm, which were higher than that (about 30%) of BST thin film directly deposited on the Pt (111). The value is comparable with that

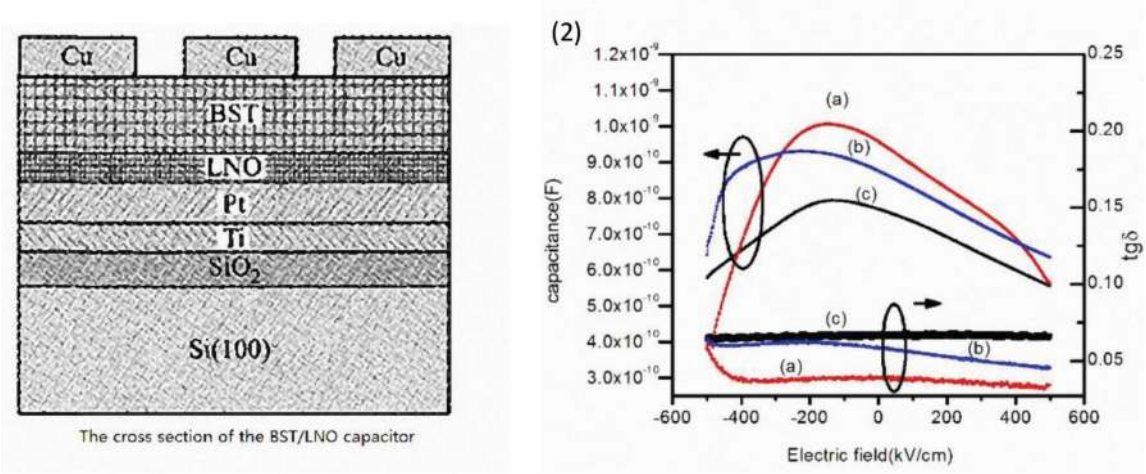

Figure 8. (1) Schematic of the capacitor, (2) the electric field dependence of dielectric property for: (a) Cu/BST/LNO (100)/Pt capacitor, (b) LNO (110)/Pt (111) and (c) Cu/BST/Pt capacitor, respectively [10].

of pulsed laser deposited BST on LNO (110)/Pt (111) (62% tunability at 262.5 kV/cm [11] and that of the BST thin film on the LNO/Pt (111) (about 51% tunability at 400 kV/cm) deposited by metal organic deposition process [12]. The results of higher capacitance are consistent with the previous structural observation, that is, the crystallization of the BST films was enhanced by LNO buffer layer. Furthermore, the dielectric loss of BST thin films was reduced for BST thin films with LNO buffer layer. It has been reported that conducting oxide like LNO aid in migration of oxygen vacancy [11], which is a possible reason for the decrease in dielectric loss of the BST thin films with LNO buffer layer. The best tunability of BST films on (100)-LNO seems to be attributed to (100) texturing of the BST films.

In addition, the effect of BST thin films thickness and post annealing on the dielectric properties of the parallel capacitor was examined. **Figure 9(a)** shows the electric field dependence of the dielectric properties of the BST thin films of different thickness with 120 nm LNO buffer layer. It should be noted that the dielectric constant did not increase with increasing thickness of BST, which is related with the interface between LNO and BST. When the LNO buffer

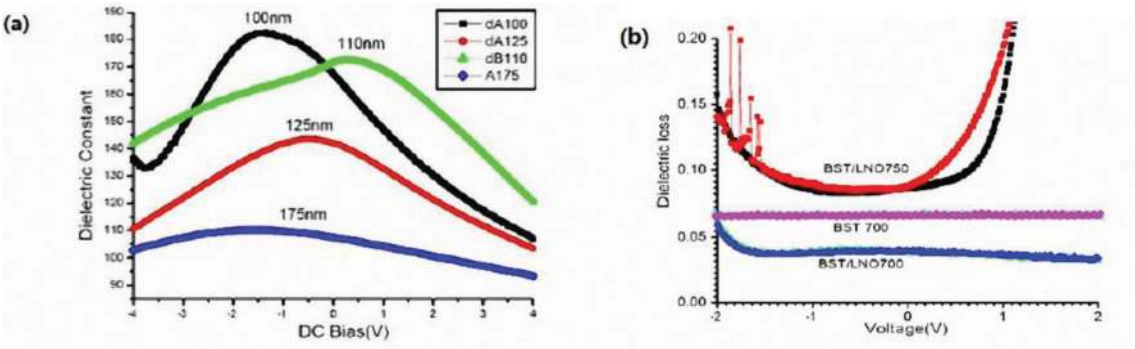

Figure 9. (a) Dielectric constant versus DC voltage with different BST thicknesses (LNO is 120 nm) and (b) the DC bias voltage dependence of dielectric loss for the thin film annealed at different temperature.

http://dx.doi.org/10.5772/intechopen.79270

layer kept 120 nm, the tunability of BST with 100–125 nm is better than that with thicker BST. **Figure 9(b)** shows the DC bias voltage dependence of dielectric loss for the thin film annealed at different temperature. It reveals that the BST/LNO/Pt/SiO_2/Si annealed at 700°C has the lowest dielectric loss, which demonstrated the LNO buffer layer help in reducing the dielectric loss. However, when the BST/LNO film was annealed at 750°C, the dielectric loss increased, and it increased rapidly with increasing bias voltage, which may be due to two reasons: one is that the Ti diffusion toward BST and reduced the effective dielectric layer, on the other hand, the lattice parameter of LNO is 3.84 and that of BST is 3.94, mismatch between BST and LNO is 2.6% the dislocations increased with increasing annealing temperature.

The effect of buffer layer thickness on the dielectric properties of the BST thin films was examined.

Figure 10(a) shows the DC bias voltage dependence of dielectric constant for the BST deposited on LNO buffer layer with varied thickness δ. The commonly used figure of merit (FOM) for electrically tuned device applications is the ratio of the tunability to dielectric loss (tgδ), the so-called K factor.

Table 3 shows the tunability and FOM of BST with different thickness of LNO buffer layer at applied electric field of 400 kV/cm. The tunability of BST thin film on the LNO (100)/Pt (111) was about 63% at a vertical applied field of 400 kV/cm, and it was higher than that (about 32%) of BST thin film on the Pt (111). **Figure 10(b)** reveals that the dielectric loss for the BST on 120 nm LNO was the smallest when the DC bias is no more than 1 V. The best dielectric properties were obtained with 120 nm LNO buffer layer, which was confirmed by microstructure examination. Many factors, such as orientation, compositions, crystallinity, strain and stress have been found to affect the dielectric properties. The crystalline quality of the LNO template layer affects the quality of BST. When the LNO was too thin, such as 60 nm, the microstructure was inhomogeneous and the crystalline quality was poor. On the other hand, too thick LNO was detrimental to the dielectric properties of BST, probably due to the interdiffusion between LNO layer and BST during long time deposition and post-annealing. The higher tunability

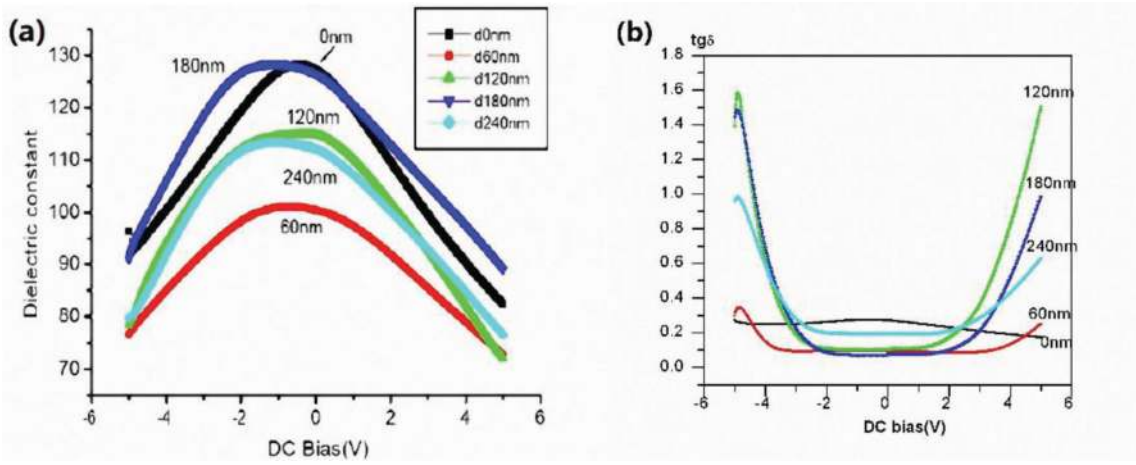

Figure 10. The DC bias voltage dependence of dielectric property for the Cu/BST/LNO/Pt capacitor of varied LNO thickness δ. (a) Dielectric constant [30] and (b) dielectric loss.

LNO under layer thickness (nm)	Tunability (%)	Figure of merit (FOM)
0	35	1.2
60	26	3.1
120	63	6.3
180	31	4.1
240	32	1.5

Table 3. The tunability and FOM of BST thin film on different thickness of LNO buffer layer.

is related to (100) texture of the BST films [30]. As a BST film subjected to tensile stress, a contraction occurred along the C axis, which leads to an enhancement of the in-plane oriented polar axis [10]. By a converse electrostrictive effect, the in-plane tensile stress reduces the capacitance in the thickness direction of the film [11]. When the (100)-oriented BST thin films were applied under higher electric fields, the in-plane orientation of the polar axis resulted in higher tunability. Hence, the tunability of (100)-oriented BST films was higher compared to the randomly oriented BST films.

3.5. BST thin film on $MgO/SiO_2/Si$ (100) substrate and its dielectric properties

Interdigital capacitor electrodes were patterned by lift-off process [31]. The thickness of electroplated Cu is about 5 μm which is larger than the skin depth of copper at 10 GHz.

3.5.1. XRD and SEM studies

MgO thin film was deposited on Si as buffer layer and its microstructure was investigated in our previous study [31]. The sputtering was carried out under room temperature, with a partial pressure of oxygen kept at 10% and the total argon and oxygen pressure of 0.3 Pa. **Figure 11a–d** shows the XRD patterns of the MgO films and BST/MgO. MgO thin film was annealed at 1000°C for the crystallization after sputtering. BST/MgO composite thin films undergo a two-step annealing process, in which the BST film was deposited on annealed MgO buffer layer (1000°C) then BST/MgO composite film was annealed at 750°C.

Figure 11(a) and **(b)** reveals that the MgO thin film deposited on (100) Si prefer to (200) orientation, but the MgO thin film on (111) Si show (111) orientation. The orientation of the BST films with and without MgO buffer layer is much different in **Figure 11c** and **d**. The MgO buffer layers enhanced the BST (100) orientation and weakened the BST (111) orientations. However, the BST/Si films did not show desirable crystal orientation when annealed at 750°C.

Furthermore, considering LNO, a kind of conductive oxide, may increase the leakage of BST on it, a thin layer of MgO (<50 nm) was inserted between LNO (100 oriented) and BST The BST was deposited on MgO/LNO bilayer and then annealed at 750°C. The microstructure of the multilayers was examined.

http://dx.doi.org/10.5772/intechopen.79270

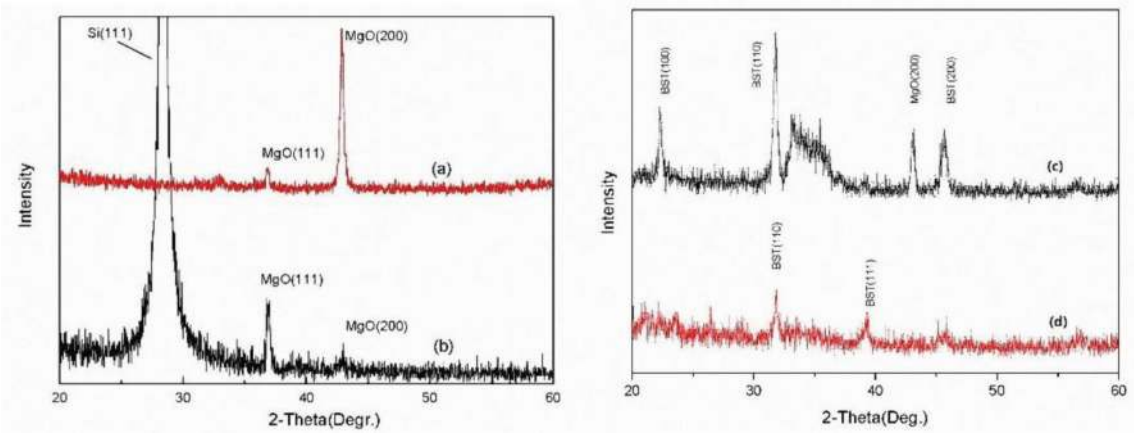

Figure 11. XRD patterns of (a) MgO films deposited on (100)Si, (b) MgO films deposited on (111) Si, (c) BST/MgO films and (d) BST/SiO_2/Si.

Figure 12(a) show that the surface of BST/MgO/LNO is smooth and the BST grain is about 15–30 nm, the XRD results in **Figure 12(b)** reveal that the BST show (100) preferential orientation and no peak of MgO was observed because MgO annealed at 750°C is still amorphous.

3.5.2. The tunable dielectrical properties of the BST thin film with and without LNO/MgO buffer layer

Figure 13 shows the tunable dielectric properties of the BST thin film with and without MgO buffer layer. The frequency is fixed at 1 MHz and the additional AC voltage is 0.05 V. The thickness of interdigital Cr/Au electrodes is about 0.5 μm, and the width of the finger is 10 μm and the gap between the fingers is 5 μm. The tunability of BST thin film without MgO buffer layer is 14.7% at 10.

V. However, the insertion of MgO buffer layer increases the tunability to 62.4% for BST/MgO (150 nm)/Si and 61.5% for BST/MgO (50 nm)/Si respectively, which is more than four times than that of BST films directly deposited on Si [31]. The dielectric loss of BST without the MgO buffer layer is about 0.1–0.15, and it decreases to about 0.05 after the insertion of the MgO buffer layer. The insertion of MgO buffer layer notably improves the tunability and at the mean time reduces the dielectric loss. The higher capacitance of BST/MgO (150 nm)/Si film compared with that of BST/MgO (50 nm)/Si film resulted from that the electrical field distribution [28] in interface (Dead layer [29]). The dead layer can reduce the dielectric capacitance of the composite films because the thinner MgO buffer layer means the more electrical distribution in the interface between Si and MgO thin film.

3.5.3. The tunable dielectrical properties of the BST/MgO/LNO multilayer

The C-V characteristic of the BST on MgO/LNO bilayer was shown in **Figure 14(a)**. For the interdigital thin film capacitor, the gap is 5 μm and the width of the finger is 5, 10, 15 μm,

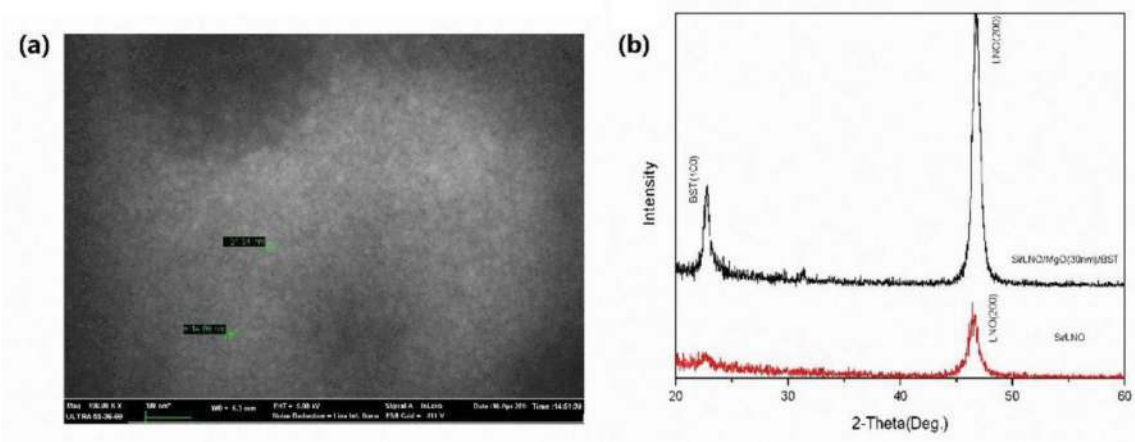

Figure 12. Characterization of the BST/MgO/LNO multilayer thin films: (a) SEM and (b) XRD patterns.

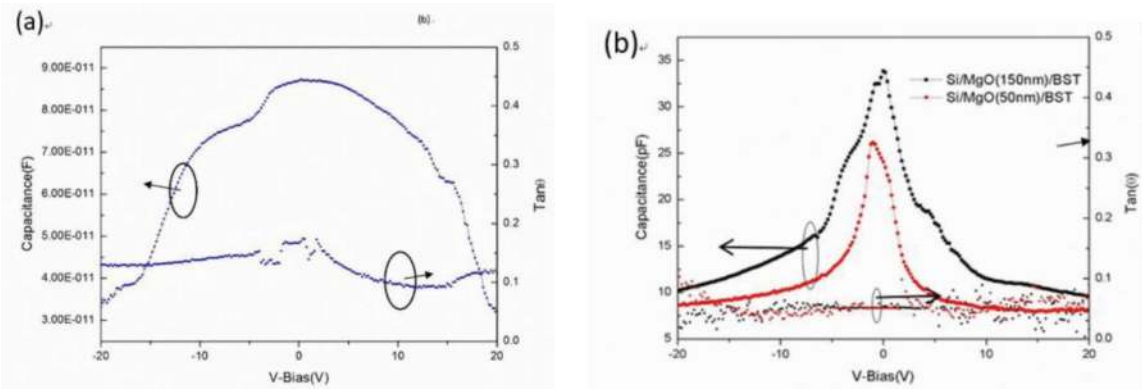

Figure 13. The dielectric properties of the BST thin film (a) without MgO; (b) on different thickness of MgO buffer layer [31].

respectively. **Figure 14(b)** reveal that the tunability of BST/MgO/LNO multilayer is higher with increasing width of the finger, but the dielectric loss also increases rapidly when the bias is larger than 15 V. Probably the interface between the multilayers resulted in the large dielectric loss at high bias voltage. Further intensive investigation is needed in order to obtain high tunability with small dielectric loss.

3.5.4. Coplanar waveguide with BST/MgO on Si substrate

Finally, coplanar waveguide (CPW) on Si substrate with BST/MgO multilayer were fabricated. The schematic of a CPW was shown in **Figure 15**, where g is the gap between the ground and signal line, w is the width of the signal line and the total of w and g is kept as constant (90 μm). To obtain the transmission and loss characteristics of the coplanar waveguide, S parameters were measured using a vector network analyzer (Agilent 8722ES). The frequency was swept from 5 to 15 GHz. The measured S-parameters of the waveguide are shown in **Figure 16**. The measured return loss S11 are lower than −40 dB at the central frequency of 10 GHz. Meanwhile, the measured S12 were close to −2.8 to −3.8 dB in measuring frequency

http://dx.doi.org/10.5772/intechopen.79270

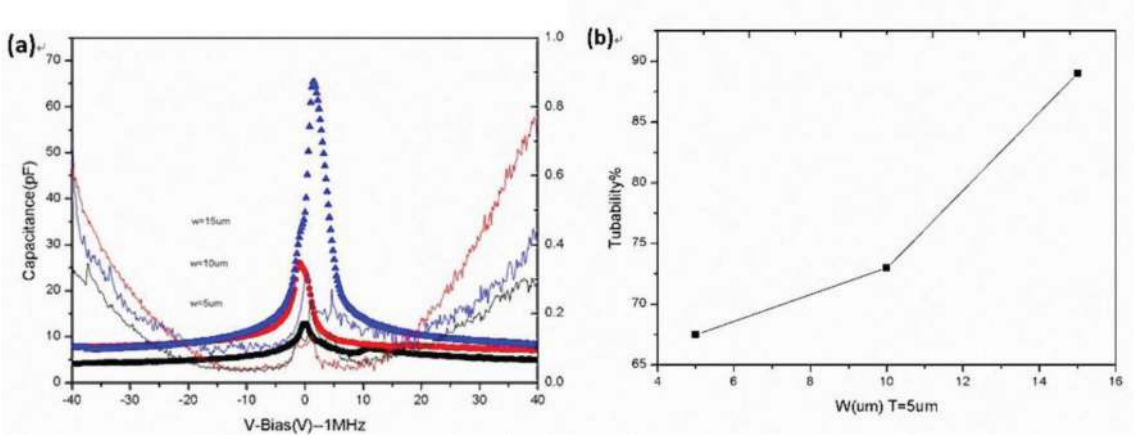

Figure 14. Dielectric property for BST/MgO/LNO interdigital capacitor with different widths of the finger (gap = 5 μm) (a) C-V curves and (b) the tunability.

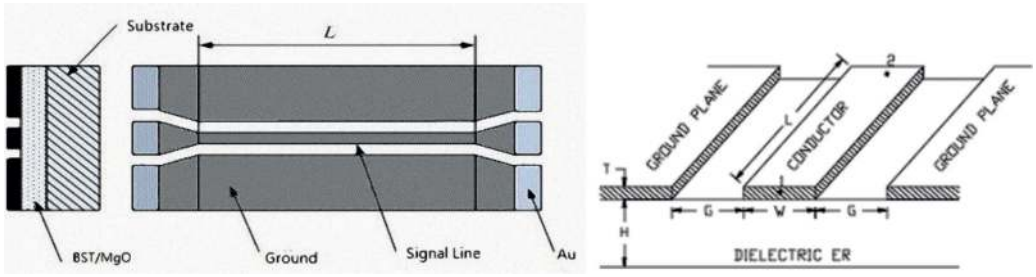

Figure 15. Schematic of a CPW with a double-layer dielectric on Si substrate.

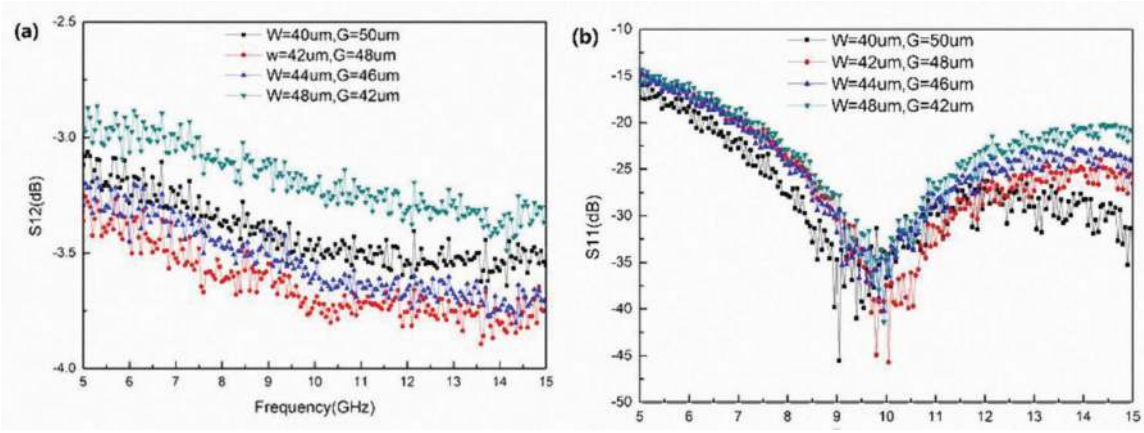

Figure 16. S parameters of the CPW with BST/MgO(w + g = 90 μm). (a) S12 and (b) S11.

band. These results indicated that the CPW based on Si substrate with BST/MgO thin films showed good transmission property near 10 GHz. It has promising application in tunable high frequency devices although the insertion loss was little higher, which need to be further optimized by design optimization of CPW and improvement of BST multilayers.

4. Conclusions

The effect of LNO/MgO buffer layer on the microstructure and dielectric properties of BST thin films was investigated. The MgO, BST and LNO films were deposited on the Si substrate by RF magnetron sputtering. It reveals that the orientation of the LNO thin films were dominated by the substrate temperature, highly (100)-oriented LNO was obtained when the substrate temperature was 300°C, and the orientation of BST thin film was tailored by the introduction of LNO buffer layer. Highly (100)-oriented $(Ba_{0.5}Sr_{0.5})TiO_3/LaNiO_3$ heterostructures were obtained on Pt(111) by RF sputtering, and LNO buffer layers enhance the growth of BST grains. The tunability were greatly improved to 63% by the introduction of (100)-textured LNO buffer layer with proper thickness, and FOM of BST thin films was also greatly improved. Also, the BST thin film interdigital capacitors were fabricated on silicon with MgO or LNO/MgO as buffer layer. The results show that insertion of the MgO buffer layer can enhance the tunability of the BST film and simultaneously reduce the dielectric loss. The MgO buffer layer can also enhance the crystallization of the BST thin films. However, LNO/MgO bilayer can greatly increase the tunability, at the same time the dielectric loss is large when the applied voltage is more than 10 V. Finally, the CPW with BST/MgO were fabricated and their S were tested, the CPW showed good transmission property near 10 GHz and showed promising application in tunable high frequency devices.

Acknowledgements

The authors would like to express their gratitude for the support from the National Natural Science Foundation of China (no. 60701012).

Author details

Congchun Zhang*, Jianze Huang, Chunsheng Yang and Guifu Ding

*Address all correspondence to: zhcc@sjtu.edu.cn

National Key Laboratory of Nano/Micro Fabrication Technology, Department of Micro/Nano Electronics, Shanghai Jiao Tong University, Shanghai, PR China

References

[1] Jia QX, Wu XD, Foltyn SR, Tiwari P. Structural and electrical properties of $Ba_0.5Sr_0.5TiO_3$ thin films with conductive $SrRuO_3$ bottom electrodes. Applied Physics Letters. 1995;**66**:2197

[2] Kim WJ, Chang W, Qadri SB, Pond JM, Kirshoefer SW, Chrisey DB, Horwitz JS. Microwave properties of tetragonally distorted $(Ba_{0.5}Sr_{0.5})TiO_3$ thin films. Applied Physics Letters. 2000;**76**:1185

[3] Zhu X, Peng HW, Miao J, Zheng DN. Fabrication and characterization of tunable dielectric $Ba_{0.5}Sr_{0.5}TiO_3$ thin films by pulsed laser deposition. Materials Letters. 2004;**58**:2045

[4] Kang BS, Lee J, Stan L, Lee JK, DePaula RF, Arendt PN. Dielectric properties of epitaxial $Ba_{0.6}Sr_{0.4}TiO_3$ films on SiO_2/Si using biaxially oriented ion-beam-assisted-deposited MgO as templates. Applied Physics Letters. 2004;**85**:4702

[5] Chu CM, Lin P. Electrical properties and crystal structure of (Ba,Sr)TiO films prepared at low temperatures on a LaNiO electrode by radio-frequency magnetron sputtering. Applied Physics Letters. 1997;**70**:249

[6] Jia QX, Wu XD, Hunng HH. Microstructure properties of Ba_0. $5Sr_0$. $5TiO_3$ thin films on Si with conductive $SrRuO_3$ bottom electrodes. Thin Solid Films. 1997;**299**:115

[7] Chen MS, Wu TB, Wu JM. Effect of textured $LaNiO_3$ electrode on the fatigue improvement of $Pb(Zr_0.53Ti_{0.47})O_3$ thin films. Applied Physics Letters. 1996;**68**:1430

[8] Chen XY, Wong KH, Mak CL, Yin XB, Liu JM, Wang M, Liu ZG. The orientation-selective growth of $LaNiO_3$ films on Si (100) by pulsed laser deposition using a MgO buffer. Applied Physics. A, Materials Science & Processing. 2002;**A75**:545

[9] Wang C, Cheng BL, Wang SY, Lu HB, Zhou YL, Chen ZH, Yang GZ. Effects of oxygen pressure on lattice parameter, orientation, surface morphology and deposition rate of $(Ba_{0.02}Sr_{0.98})TiO_3$ thin films grown on MgO substrate by pulsed laser deposition. Thin Solid Films. 2005; **485**:82

[10] Zhang CC, Shi JC, Yang CS, Ding GF. Preparation of (1 0 0)-oriented $LaNiO_3$ on Si for the textured Ba_0. $5Sr_0$. $5TiO_3$ thin films. Applied Surface Science. 2008;**255**:2773-2776

[11] Tang XG, Xiong HF, Jiang LL, Chan LHW. Dielectric properties and high tunability of (1 0 0)-and (1 1 0)-oriented (Ba_0. $5Sr_{0.5}$) TiO_3 thin films prepared by pulsed laser deposition. Journal of Crystal Growth. 2005;**285**:613-619

[12] Gao YH, Sun JL, Ma JH, et al. Improved dielectric and electrical properties of $(Ba,Sr)TiO_3$ thin films using Pt/$LaNiO_3$ as the top-electrode material. Applied Physics. A, Materials Science & Processing. 2008;**91**(3):541-544

[13] Yoon HK, Sohn JH, Lee BD, Kang DH. Effect of $LaNiO_3$ interlayer on dielectric properties of $(Ba_0.5Sr_{0.5})TiO_3$ thin films deposited on differently oriented Pt electrodes. Applied Physics Letters. 2002;**81**:5012

[14] Chun YH, Hong JS, Peng B, Jackson TJ, Lancaster MJ. An Electronically Tuned Bandstop Filter Using BST Varactors. Microwave Conference, EuMC, 38th European. 2008. pp. 1699-1702

[15] Jia JF, Huang K, Pan Q, He DY. Significant suppression of leakage current in (Ba x ,Sr_1-x)TiO_3/MgO heterostructured thin films by thin MgO layers insertion. Journal of Sol-Gel Science and Technology. 2007;**42**(1):9-12

[16] Yoon YK, Kenney JS, Hunt AT, Allen MG. Low-loss microelectrodes fabricated using reverse-side exposure for a tunable ferroelectric capacitor application. Journal of Micromechanics and Micro-engineering. 2006;**16**(2):225-234

[17] Liu SS, Ma BH, Narayanan M, Chao S, Koritala R, Balachandran U. Improved properties of barium strontium titanate thin films grown on copper foils by pulsed laser deposition using a self-buffered layer. Journal of Physics D: Applied Physics. 2012;**45**(6pp):175304

[18] Yan DX, Xu ZP, Chen XL, Xiao DQ, Yu P, Zhu JG. Microstructure and electrical properties of Mn/Y codoped $Ba_{0.67}Sr_{0.33}TiO_3$ ceramics. Ceramics International. 2012;**38**:2785-2791

[19] Kwon SR, Huang WB, Zhang SJ, Yuan FG, Jiang XN. Flexoelectric sensing using a multilayered barium strontium titanate structure. Smart Materials and Structures. 2013; **22**:115017

[20] Iskandar J, Syafutra H, Juansah JJ, Irzaman. Characterizations of electrical and optical properties on ferroelectric photodiode of barium strontium titanate ($Ba_{0.5}Sr_{0.5}TiO_3$) films based on the annealing time differences and its development as light sensor on satellite technology. Procedia Environmental Sciences. 2015;**24**:324-328

[21] Hu SD, Li H, Tzou HS. Distributed flexoelectric structural sensing: Theory and experiment. Journal of Sound and Vibration. 2015;**348**:126-136

[22] Kwon SR, Huang W, Shu L, Yuan FG, Maria JP, Jiang X. Flexoelectricity in barium strontium titanate thin film. Applied Physics Letters. 2014;**105**:142904

[23] Nam SH, Lee WJ, Kim HJ. Oriented growth of SrTiO, thin films on Si substrate by radio frequency I magnetron sputtering. Journal of Physics D: Applied Physics. 1994;**27**:866-870

[24] Song TK, Ahn JS, Choi HS, Noh TW, Kwun SI. Infrared properties of epitaxial $SrTiO_3$ thin films on MgO(001) substrates. Journal- Korean Physical Society. 1997;**30**(3):623-627

[25] Yang YF, Nordman JE, Lee JU. Effects of deposition conditions on stoichiometry of off-axis RF sputtered BiSrCaCuO thin films. IEEE Transactions on Applied Superconductivity. 1993;**3**:1543-1546

[26] Zhang C, Hou J, Rao R, Yang C, Ding G. Effects of process parameters on the $LaNiO_3$ thin films deposited by radio-frequency magnetron sputtering. Thin Solid Films. 2009;**517**:6837-6840

[27] Zhang CC, Shi JC, Yang CS. Effect of Sputtering Process on Structure of $LaNiO_3$ Thin Films. Journal of Functional Materials and Devices. 2008;**14**(1):215-217

[28] Kim DY, Lee SG, Park YK, Park SJ. Effect of ambient gas pressure on the preferred orientation of barium titanate thin films prepared by pulsed laser deposition. Japanese Journal of Applied Physics. 1995;**34**:L1564

[29] Hu LY, Fu CR, Yang CL. Study on the Asymmetry of C-V Curves in Barium Titanate Thin Films. Journal of Functional Materials. 2005;**36**(11):1704-1705

[30] Zhang CC, Yang CS, Shi JC, et al. Effect of $LaNiO_3$ Interlayer on the Dielectric Properties of $Ba_{0.5}Sr_{0.5}TiO_3$ Thin Film on Si Substrate. Journal of Shanghai Jiaotong University. 2009;**14**(2):133-136

[31] Hou J, Zhang C, Yang C, Ding G. High tunable $Ba_{0.5}Sr_{0.5}TiO_3$ thin film deposited on silicon substrate with MgO buffer layer. International Journal of Nanomanufacturing. 2011; **7**(5/6):567-574